International Forum on Aeroelasticity and Structural Dynamics
IFASD 2024
17-21 June 2024, The Hague, The Netherlands

HIGHLY FLEXIBLE AIRCRAFT FLIGHT DYNAMICS SIMULATION USING CFD

Alain Dugeai[1], Pierre Vuillemin[2]
[1] DAAA, ONERA, Institut Polytechnique de Paris
92320 Châtillon, France
[2] DTIS, ONERA, Université de Toulouse
31000 Toulouse, France

Keywords: Aeroelasticity, fluid-structure coupling, flexible aircraft, flight dynamics, control, gust response, GLA, maneuver, CFD.

Abstract: The present paper focuses on the development of a numerical CFD methodology for the simulation of the flight dynamics of the flexible aircraft, in open loop and in closed loop as well. To do so, a modular environment is developed to couple the ONERA CFD solver elsA with Python modules implementing several simulation capabilities: prescribed complex trajectory, 6 DoFs flight dynamics, structural linear dynamics, control surfaces actuations, control laws. The basic assumptions and numerical features of the developed environment are presented along with a reminder of the unsteady deformable capabilities of the elsA code, and several applications performed in the frame of the French DGAC funded MAJESTIC project on the HAR XRF1 configurations are shown. In particular the topic of the simulation of active Gust Load Alleviation is examined. Perspectives are given on the future extension of the approach to the accounting for non-linear structural behaviour, and the possible use of other CFD solver such as CODA or the ONERA next generation solver SoNICS.

Nomenclature:

X_G: coordinates of the center of gravity in inertial frame
ω^b: rotation rate in body axes, (p, q, r): components of the rotation rate vector
(F_x, F_y, F_z): components of the external forces, m: mass
(M_x, M_y, M_z): components of the moments of external forces, J: inertia matrix
K:stiffness matrix, M: mass matrix, ω: pulsation, f: frequency, ϕ: modal basis
q: generalized coordinates, γ: generalized stiffness, μ: generalized mass
α: angle of attack, δ: HTP deflection angle

1 INTRODUCTION

The next generation of civil aircraft will have to be technically performing and ecologically friendly. One main issue is the reduction of the environmental footprint of aviation, through CO2 emission and fuel consumption reduction. To do so, several levers may be operated. The mains are the improvement in engine efficiency, green fuel, mass optimization using innovative materials, and also aircraft shape optimization.

Considering shape optimization, the main option is an increase of the wing span, in order to reduce the lift induced drag. This long term trend of aspect ratio increase is presented on Figure 1 which compares the lift over drag ratio (L/D) to the wing aspect ratio (AR). An increase in aspect ratio is clearly related to drag gains.

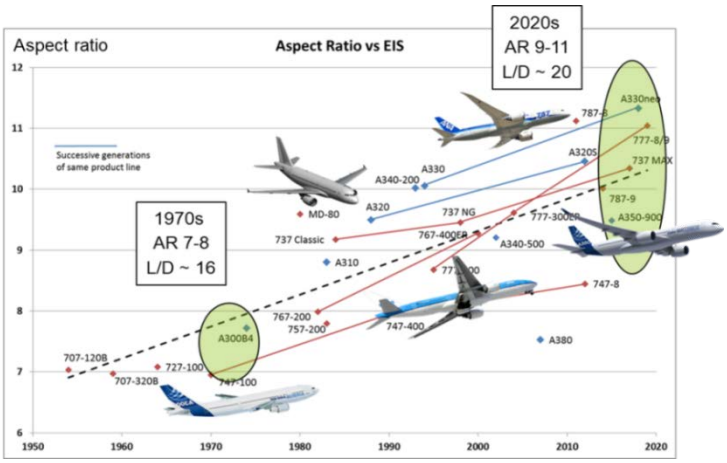

Figure 1 Civil aircraft wing aspect ratio evolution

However, increasing the wing aspect ratio leads to structural design and aeroelastic issues. Indeed, a larger wing span induces higher loads (bending moments) at wing root, which have to be sustained by a structural reinforcement leading to an increase in mass. In turn, this mass penalty is likely to induce drag penalty. Therefore, increasing the wing flexibility becomes mandatory, in order to reduce mass, while sustaining the higher loads.

But the implementation of a highly flexible wing needs to carefully analyse the aeroelastic behaviour of the aircraft. In static, high levels of vertical deflection and twist may be reached, which must be considered in the design, for the whole flight envelope. In dynamic, increased flexibility may be responsible for flutter issues, high levels of dynamic response to manoeuvre or gust, which must be carefully cleared. Moreover, increased flexibility leads to lower structural modes frequencies, which may induce coupling with flight dynamics and control laws frequencies. Eventually, the wing structure may be flexible enough to require a non-linear formulation to properly model large displacements.

The topic of the flight dynamics of the flexible aircraft has been studied by a number of authors. Among them, C. Cesnik from University of Michigan has been working for years on the topic. Collaboration with R. Palacios from Imperial College London recently lead to the publication of a handbook on the topic (Palacios [1]). In this book, the fundamentals of flight dynamics and structural dynamics are exposed, as well as the various assumption levels for the coupling of both disciplines. However, the topic of the coupling of CFD in the time domain is not covered in this book, where only low fidelity aerodynamics is considered (DLM, VLM, UVLM).

In Nguyen [2], the authors develop the formulation for a flexible aircraft, considering a beam model of the wing coupled with rigid-body motions of the aircraft. Aeroelastic effect are taken into account using Theodorsen unsteady airfoil theory.

Murua [3] investigate the gust response in open-loop and closed loop of an unmanned flexible aircraft. The equations are firstly derived in the case of large displacements using a non-linear beam model and the linearized for stability analysis. The aerodynamic modelling is base on a vortex-lattice model solved in the time domain. Linear controllers are included in the loop, in order to evaluate GLA capabilities on the HALE configuration.

V. Portapas from Cranfield University presents in [4] an overview of the capabilities of the CA2LM framework. In this work aerodynamic forces are computed using steady and unsteady

strip theory approaches. More recently in its PhD thesis Pau-Castells examines in transonic the use of CFD-LFD (Linearized Frequency Domain) for the generation of an RFA (Rational Function Approximation) reduced model of the generalized unsteady aerodynamic forces in the case of the gust response of a civil aircraft.

Considering CFD approaches, they have been implemented for gust response simulations by Heinrich in [5] at DLR. The same team (Ritter [6]) has more recently applied CFD to flight dynamics maneuvers using TAU code in a Virtual Flight Test numerical environment.

In transonic, and for complex aircraft structures, the use of more sophisticated aerodynamic models has indeed to be considered for analysing the flight dynamics of flexible aircrafts. In this paper, we evaluate the use of CFD in the transonic regime for the resolution of the flexible aircraft flight dynamics, including gust response, in the case of a realistic long-range civil aircraft model.

2 NUMERICAL METHODOLOGY

A large number of numerical features are necessary to address flexible flight dynamics simulations using CFD in time domain. First of all, a CFD solver capable of unsteady flexible simulation is to be implemented. In this work, the elsA ONERA solver has been used. The main characteristics of the solver are detailed below, especially those which are mandatory for the targeted simulations. Besides the solver, a modular framework has been developed in order to couple the different features involved in these simulations:

- Rigid aircraft flight dynamics module;
- Structural dynamics solver;
- Control surfaces actuation capability;
- Mesh deformation;
- Trim capabilities;
- Gust modelling;
- Control laws.

These different components are described in the following sections. A specific point is devoted to the description of the assumptions leading to the decoupling of flight dynamics and structural dynamics equations.

2.1 elsA solver features

elsA is the ONERA software for complex external and internal flow simulations and for multi-disciplinary applications involving aerodynamics (Cambier [7,8]). This covers the following disciplines and topics:

- Aerodynamics, aeroelasticity, aerothermics coupling, aeroacoustics coupling;
- Aircrafts, helicopters, turbomachinery, missiles, launchers, air intakes, nozzles, propulsive jets;
- Research and industrial applications;
- Euler, RANS, URANS, DES, LES simulations;
- Calculation of sensitivities for optimum design.

2.1.1 Moving/Flexible grid capabilities of the elsA solver

Motions and deformations of bodies may be taken into account in elsA for steady/unsteady applications (Dugeai [9]). Mesh deformation is allowed in dynamic using an ALE formulation of flow equations. Flow equations may either be described in a moving frame (implementing entrainment velocities) or in the fixed frame, where motion or deformation may be implemented by the prescription of grid velocities and the update of grid coordinates. In this case, which is the one adopted here for the presented simulations, boundary conditions must be adapted to cope with the local motion.

Recently, the aeroelastic features of the solver have been extended by the capability of externalizing the mesh deformation step. In this approach, for unsteady moving/deformable simulations, the CFD grid (and the grid velocity as well) is prescribed to the CFD solver at each physical time step by an external Python module. This feature allows a much more user-friendly framework for the potential extension to a large range of unsteady flexible simulations. Indeed, in the case of aeroelastic coupling, aerodynamic loads are extracted at each time step and may be provided to a flight dynamics solver and in the flexible case, to a structural dynamics solver. In the rigid case, this feature has been used for the purpose of generating a ROM of the aerodynamic coefficients of a generic UCAV configuration, using CFD simulations of complex unsteady prescribed motions of the model (Isnard [10], Figure 2). In the present work, we extend this feature to the resolution of the flight dynamics of flexible models.

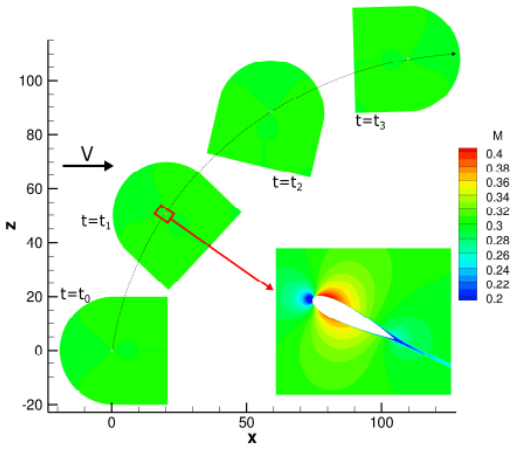

Figure 2 : Constant pitch rotation rate CFD simulations of a Naca airfoil

2.2 Flight dynamics model

Flight dynamics equations describe the motion of the center of mass and of the evolution of the attitude of the aircraft (currently given by Euler angles) in the inertial ground frame of reference. Newton laws are applied for translation and rotation components. Translation equations are generally written in the inertial frame, whereas rotation equations are usually written in the body axes, and implement the rotation rates components (p, q, r) and inertia matrices given in the body frame.

The center of mass motion equations are written in the inertial frame as:

$$m\ddot{X}_G = F_a^i + F_p^i + F_g^i \qquad (2.2.1)$$

where the forces acting on the system may include aerodynamic, propulsion and gravity forces, expressed in the inertial frame.

Rotation motion equations may be written (Caughey [11]), considering the body frame to be the inertia principal axes frame:

$$\begin{cases} M_x^b = I_x\dot{p} + \left(I_z - I_y\right)qr \\ M_y^b = I_y\dot{q} + (I_x - I_z)rp \\ M_z^b = I_z\dot{r} + \left(I_y - I_x\right)pq \end{cases} \qquad (2.2.2)$$

with

$$D = \begin{pmatrix} 0 & -r & q \\ r & 0 & -p \\ -q & p & 0 \end{pmatrix} \qquad J = \begin{pmatrix} I_x & 0 & 0 \\ 0 & I_y & 0 \\ 0 & 0 & I_z \end{pmatrix} \qquad \omega^b = \begin{pmatrix} p \\ q \\ r \end{pmatrix} \qquad \vec{M}^b = \begin{pmatrix} \mathrm{M_x^b} \\ \mathrm{M_y^b} \\ \mathrm{M_z^b} \end{pmatrix}$$

The rotation rate evolution equation comes:

$$\dot{\omega}^b = J^{-1}\left(\vec{M}^b - D.J.\omega^b\right) \qquad (2.2.3)$$

This equation may be written in an elegant way using the quaternion $Q = (e_0, e_1, e_2, e_3)$ (Murman [12]) describing the attitude of the aircraft by:

$$\dot{Q} = \frac{1}{2}\ {}^{T}L\ \omega^b \qquad {}^{T}L(Q) = \begin{pmatrix} -e_1 & -e_2 & -e_3 \\ e_0 & -e_3 & e_2 \\ e_3 & e_0 & -e_1 \\ -e_2 & e_1 & e_0 \end{pmatrix} \qquad (2.2.4)$$

Note that using quaternions in the flight dynamics equations has a triple advantage:

- it relieves the singularity of Euler angles at pitch angle 90°;
- it allows a more robust numerical resolution with respect to the matrix formulation;
- it allows a more compact (4 terms) description of the orientation of the aircraft axes wrt matrices (9 terms).

Introducing the flight dynamics state variable $W = {}^{T}\left(\dot{X}_G, X_G, \omega^b, Q\right)$ the problem may be formulated using a first order in time ODE:

$$\frac{dW}{dt} = F(W) \qquad (2.2.5)$$

Where flux F is given by:

$$F(W) = \begin{pmatrix} \frac{1}{m}\overrightarrow{F^i} \\ 0 \\ J^{-1}\vec{M}^b \\ 0 \end{pmatrix} + \begin{pmatrix} O_3 & O_3 & O_3 & O_{3,4} \\ I_3 & O_3 & O_3 & O_{3,4} \\ O_3 & O_3 & -J^{-1}D.J & O_{3,4} \\ O_{4,3} & O_{4,3} & \frac{1}{2}\ {}^{T}L & O_4 \end{pmatrix} W \qquad (2.2.6)$$

This equation may be solved using a numerical integration scheme where mechanical terms are implicited.

During the time domain flight dynamics simulation, the aerodynamic forces and moments $\overrightarrow{F^i}$ and $\vec{M}^b$ depends on the flight dynamics state W resulting in a coupling between flight dynamics equations and aerodynamics. Therefore, in order to solve the flight dynamics/aerodynamics coupling, a fixed-point loop is to be implemented to ensure the unsteady equilibrium.

2.3 Flight dynamics of the flexible model

In this paper, the structural model is considered to stay linear. Therefore, a projection of the mechanical equations on the free-free modes of the structure is performed.

The free-free modal basis is obtained solving the classical eigen value problem

$$(K - \omega^2 M)X = 0 \qquad (2.3.1)$$

where K is the unconstrained stiffness matrix of the structure, M the mass matrix, and X the physical displacement vector of the structure. Due to the lack of constraints, the stiffness matrix is singular and the system exhibits in general 6 rigid modes with zero eigen value (internal mechanisms may introduce additional rigid modes, but this case will not be considered here).

Hence, the free-free modal basis ϕ may be written $\phi = (\phi_R, \phi_S)$ where ϕ_R stands for the 6 rigid modes which happens to be combinations of the 3 free translations and the 3 free rotations of the model, and ϕ_S a certain number N_S of flexible modes. As explained, the rigid modes are associated to a zero eigen value, which corresponds to a null frequency. The K is therefore singular of dimension $N_S + 6$ and of rank N_S, and we have $K\phi_R = 0$.

Considering the classical structural dynamics equations in the body frame we have:

$$M\ddot{X} + KX = F_{tot} \qquad (2.3.2)$$

Note that F_{tot} may include additional terms due to rotation (centrifugal, Coriolis), if the body frame is accelerated wrt the Galilean reference frame.

If we project the structural dynamics equations on the free-free modal basis, introducing the physical displacement decomposition on modal basis ϕ as follows

$$X = \phi q = (\phi_R, \phi_S)\begin{pmatrix} q_R \\ q_S \end{pmatrix} \qquad (2.3.3)$$

we obtain:

$$\begin{pmatrix} {}^t\phi_R \\ {}^t\phi_S \end{pmatrix} M(\phi_R, \phi_S)\begin{pmatrix} \ddot{q_R} \\ q_S \end{pmatrix} + \begin{pmatrix} {}^t\phi_R \\ {}^t\phi_S \end{pmatrix} K(\phi_R, \phi_S)\begin{pmatrix} q_R \\ q_S \end{pmatrix} = \begin{pmatrix} {}^t\phi_R \\ {}^t\phi_S \end{pmatrix} F_{tot} \qquad (2.3.4)$$

and due to the properties of orthogonality of M and K with respect to the modal basis, and that of zero stifness of the rigid modes we have:

$$\begin{pmatrix} {}^t\phi_R M\phi_R & 0 \\ 0 & {}^t\phi_S M\phi_S \end{pmatrix}\begin{pmatrix} \ddot{q_R} \\ q_S \end{pmatrix} + \begin{pmatrix} 0 & 0 \\ 0 & {}^t\phi_S K\phi_S \end{pmatrix}\begin{pmatrix} q_R \\ q_S \end{pmatrix} = \begin{pmatrix} {}^t\phi_R \\ {}^t\phi_S \end{pmatrix} F_{tot} \qquad (2.3.5)$$

Introducing the generalized mass and stiffness matrices μ and γ, the system may be written:

$$\begin{cases} \mu_R \ddot{q_R} - {}^t\phi_R F_{tot} = 0 \\ \mu_S \ddot{q_S} + \gamma_S q_S - {}^t\phi_S F_{tot} = 0 \end{cases} \qquad (2.3.6)$$

At this point several points must be made:

- The upper part of above equation corresponds to the linearization of flight dynamics equations described in §2.2. μ_R corresponds to the projection of the mass and inertia matrices on the ϕ_R base, which is a combination of pure translation/rotation modes.
- If the mechanical properties (stiffness and mass matrices and modes) are supposed to be constant, the coupling between flight dynamics (upper equation) and structural dynamics (lower equation) only occurs through the external forces F_{tot}
- External forces F_{tot}, depends on the state of the flexible system, which includes $q_R, \dot{q_R}$ (linerization of the flight dynamics state variables W of §2.2) and $q_s, \dot{q_s}$, generalized coordinates of the projected structural dynamics system.

2.4 Structural dynamics equations in the moving body frame

The structural dynamics equations projection on the flexible free-free modes is now written:

$$\mu_S \ddot{q_S} + \gamma_S q_S = {}^t\phi_S F_{tot} \qquad (2.4.1)$$

This equation is written in the moving body frame. Doing so, it's mandatory to consider additional force terms due to acceleration of the body frame with respect to the Galilean reference frame: Coriolis acceleration, and entrainment acceleration. Therefore, right hand side forces exhibit the following components: aerodynamics, gravity, propulsion, Coriolis and entrainment forces:

$$F_{tot} = F_a + F_g + F_p + F_{Cor} + F_{entr} \qquad (2.4.2)$$

Let's first show that gravity forces and uniform (not depending on spatial location) acceleration forces do not act on free-free flexible modes:

$${}^t\phi_S F_g = \int_\Omega \vec{g}.\vec{\phi}_S \, \rho(M) \, d\Omega = \vec{g}.\int_\Omega \vec{\phi}_S \, \rho(M) \, d\Omega = 0 \qquad (2.4.3)$$

due to the fact that flexible modes are orthogonal wrt to mass to rigid modes, which includes translation constant shapes ($\int_\Omega \vec{\phi}_S \, \rho(M) \, d\Omega = 0$)

In this paper we will neglect the effect of Coriolis acceleration ($F_{Cor} = 0$). Considering the entrainment acceleration, it is made of three terms, the first one being due to the acceleration of the origin B of the body frame. This term is uniform and its projection on flexible free-free modes vanishes just like uniform gravity forces. The second one is due the rotation acceleration $\frac{d\vec{\omega}}{dt}$ and will be neglected. The third term is the centrifugal term $\vec{\omega} \times \left(\vec{\omega} \times \overrightarrow{\mathrm{B}M}\right)$. In this paper we will only consider uniform acceleration maneuver (which means large radius of curvature of the trajectory compared to the aircraft dimensions), which excludes large rotation rates motions). These maneuvers are then considered as generating additional loads factor (2.5g for example). In this case, the projection of the centrifugal force field on flexible free-free modes also vanishes just as shown above.

Eventually, the projection of the total forces acting on the aircraft in the body frame reduces to that of aerodynamics and propulsion forces:

$${}^t\phi_S F_{tot} = {}^t\phi_S F_a + {}^t\phi_S F_p$$

Considering zero axial acceleration of the aircraft, propulsion forces are balanced by the axial drag aerodynamic force.

2.5 Summary of the assumptions made

Assumptions which will hold for the current paper simulations presented below are now summarized:

- The dynamic deflections of the structure are limited enough to consider a constant inertia matrix.
- Flight dynamics equations are solved keeping the non-linear §2.2 equations, instead of the linearized version obtained by modal projection §2.3
- Modal equations of eq. 2.3.6, lower are solved for structural dynamics
- Coriolis acceleration may be neglected in the solving of structural dynamics equations
- Rotation acceleration entrainment forces may be neglected
- Centrifugal forces are only due to uniform acceleration maneuver
- Propulsion forces are balancing drag axial forces (no axial acceleration)
- Due to the previous 4 points, only lateral and vertical aerodynamic forces are to be considered in the right-hand side of free-free modal structural dynamics equations (2.4.1)

3 TRIM SIMULATION

In order to perform aircraft flight dynamics simulations for maneuver or gust response, it's first necessary to obtain the static equilibrium of the aircraft. Therefore, considering symmetry of the aircraft, a longitudinal trim simulation is performed in order to balance weight vs lift and get zero pitching aerodynamic moment. This goal is reached by tuning simultaneously the angle of attack of the aircraft and the deflection angle of the horizontal tail plane. This section presents the numerical methodology developed for CFD trimmed simulations.

3.1 Residual formulation

The static equilibrium is written as

$$\begin{cases} F_z = F_{z\_tgt} \\ M_y = 0 \end{cases} \qquad (3.1.1)$$

With α being the angle of attack and δ the HTP deflection angle, we define the trim variable

$$T = \begin{pmatrix} \alpha \\ \delta \end{pmatrix}$$

The trim problem may be written in residual form:

$$R(T) = 0 \qquad R(T) = \begin{pmatrix} F_z(T) - F_{z\_tgt} \\ M_y(T) \end{pmatrix}$$

This non-linear problem could be solved using a Newton-like method, which needs the aerodynamic jacobian matrix $\frac{\partial R}{\partial T}$**.** In this paper, the resolution of the trim problem is performed using a structural dynamics system-like dynamic problem:

$$\mu \ddot{T} + \beta \dot{T} = R(T) \qquad (3.1.2)$$

which reduces to $R(T) = 0$ at static convergence. Let T_s be the solution of the trim problem ($R(T_s) = 0$) and $\tau = T - T_s$ the offset to T_s variable, we may split residual $R(T)$ in highlighting its linear and non-linear ($R_{NL}(\tau)$ with $R_{NL}(0) = 0$) contributions:

$$R(T) = R(T_s) + \frac{\partial R}{\partial T}\tau + R_{NL}(\tau) = \frac{\partial R}{\partial T}\tau + R_{NL}(\tau)$$

The dynamic equations for the offset τ is written:

$$\mu\ddot{\tau} + \beta\dot{\tau} - \frac{\partial R}{\partial T}\tau = R_{NL}(\tau) \qquad (3.1.3)$$

where $\frac{\partial R}{\partial T}$ may be seen as an aerodynamic stiffness matrix given by:

$$\frac{\partial R}{\partial T} = \begin{pmatrix} \frac{\partial F_z}{\partial \alpha} & \frac{\partial F_z}{\partial \delta} \\ \frac{\partial M_y}{\partial \alpha} & \frac{\partial M_y}{\partial \delta} \end{pmatrix} \qquad (3.1.4)$$

These terms correspond to the dimensioned forces classically obtained via the flight dynamics aerodynamic coefficients ($C_{z\alpha}$, $C_{z\delta}$, $C_{m\alpha}$, $C_{m\delta}$).

3.2 Resolution of the trim equation

The aim of the dynamic approach proposed in the previous section for the resolution of trim equations is to get a solution quickly converging to the static equilibrium without altering the aerodynamic stiffness of the system. Therefore, mass μ and damping β in eq. (3.1.1) must be properly tuned to get:

- high characteristic frequency f_{tgt} of the system wrt to simulation duration T, i.e. $f_{tgt} \ll \frac{1}{T}$
- high damping value leading to an aperiodic behavior of the dynamic system,

in order to obtain a reduction of the desired number of orders of magnitude of the residual $R(T)$ during the time domain simulation.

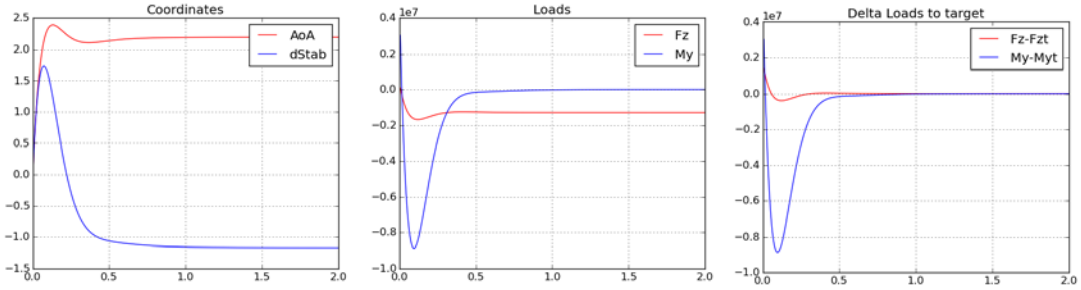

Figure 3 : Example of dynamic resolution of a simplified test model trim problem

Hence, masses and damping values are selected as follows, considering for simplification only diagonal terms of the jacobian matrix $\frac{\partial R}{\partial T}$:

$$\mu_\alpha = -\frac{\partial F_z}{\partial \alpha}/\left(2\pi\, f_{tgt}\right)^2 \qquad \mu_\delta = -\frac{\partial M_y}{\partial \delta}/\left(2\pi\, f_{tgt}\right)^2 \qquad (3.2.1)$$

$$\beta_\alpha = coef * 2\sqrt{-\frac{\partial F_z}{\partial \alpha}\mu_\alpha} \qquad \beta_\delta = coef * 2\sqrt{-\frac{\partial M_y}{\partial \delta}\mu_\delta} \qquad (3.2.2)$$

Simple assumptions on $C_{z\alpha}$ and $C_{m\delta}$ provides approximate values for aerodynamic sensitivities $\frac{\partial F_z}{\partial \alpha}$ and $\frac{\partial M_y}{\partial \delta}$ able to drive the scheme to the trim solution (example shown on Figure 3).

4 MESH DEFORMATION

The simulation of flight dynamics problems in the case of a flexible model needs to face two different problems of model deformation:

- Mesh deformation due to flexibility
- Geometry modification due to the actuation of control surfaces

In this paper, both are addressed using mesh deformation techniques.

4.1 Control surface actuation

The exact accounting for control surface actuation in the CFD grid is a complex problem, which may be addressed using several techniques:

- Mesh deformation
- Sliding meshes along the fuselage or in a fluid gap;
- Overset grid techniques,
- Immersed boundaries (IBM).

The simplest method which does not imply mesh connectivity modification is the mesh deformation technique. Indeed, it faces several drawbacks: 1) fluid gap flow not represented, 2) deformation smoothing mandatory, 3) amplitude of deflections limited. However, due to its simplicity, this method will be used in this paper (the approach could be improved in future works).

As explained above, the smoothing of the control surface deflection has to be performed. To do so, a convolution of the exact surface motion (rotation about the hinge) with a RBF Gaussian kernel function G_ρ of tunable characteristic radius ρ is performed (Figure 4). This allows the smoothing of the deflection function over a distance fitting the control surface dimension.

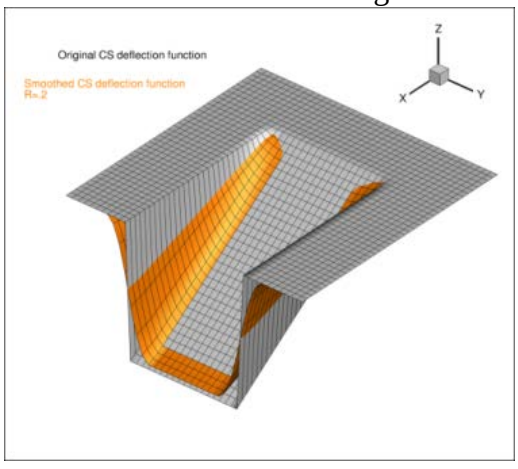

Figure 4 : Smoothing by convolution with a Gaussian kernel

A cartesian surface working grid ($x_j^{(1)}$) is built where the theoretical motion $u\left(x_j^{(1)}\right)$ is computed and the smoothing over the surface aerodynamic grid ($x_i^{(2)}$) is computed by the following convolution formula:

$$u\left(x_i^{(2)}\right) = \frac{\sum_j u\left(x_j^{(1)}\right) G_\rho(\left|x_i^{(2)} - x_j^{(1)}\right|)}{\sum_j G_\rho(\left|x_i^{(2)} - x_j^{(1)}\right|)} \qquad (4.1.1)$$

where the Gaussian kernel is written:

$$G_\rho(r) = e^{-\left(\frac{r}{\rho}\right)^2}$$

4.2 3D CFD mesh deformation

Several mesh deformation techniques may be applied:

- Elastic analogy (spring technique or continuous medium);
- Transfinite interpolation (for structured grids);
- Inverse Distance Weighting;
- Quaternion propagations;
- Radial Basis Functions based techniques (RBF).

In this paper, the solver Quantum, which uses a quaternion-based propagation technique via Inverse Distance Weighting has been implemented for control surfaces deflected deformed mesh generation, due to its robustness. This code is parallelized, and optimized using FMM (Fast Multipole Method). For the smoother deformation corresponding to structural modal deformation, a classical RBF technique (available in scipy) is used.

All the 3D mesh deformations are computed in a pre-processing step, and stored in the CGNS compliant CFD data base. Assuming linearity of the mesh deformation, they are linearly recombined on the fly during the time domain CFD simulations, from the values of the angular deflections of control surfaces and that of the generalized modal coordinates.

5 MODULAR IMPLEMENTATION

An overview of the modular framework implemented for elsA in the case of the close loop gust response is shown on Figure 5. An application in the case of the XRF1 model of the project MAJESTIC will be presented in the applicative section of this paper. The elsA solver is used as CFD solver, in externalized mode, which means that mesh and grid velocity updates may be provided at each time step from external modules. Figure 5 depicts the modular environment implemented in the case of the gust response of the flexible aircraft in closed loop, used for the Gust Load Alleviation (GLA) simulation presented in section 6.

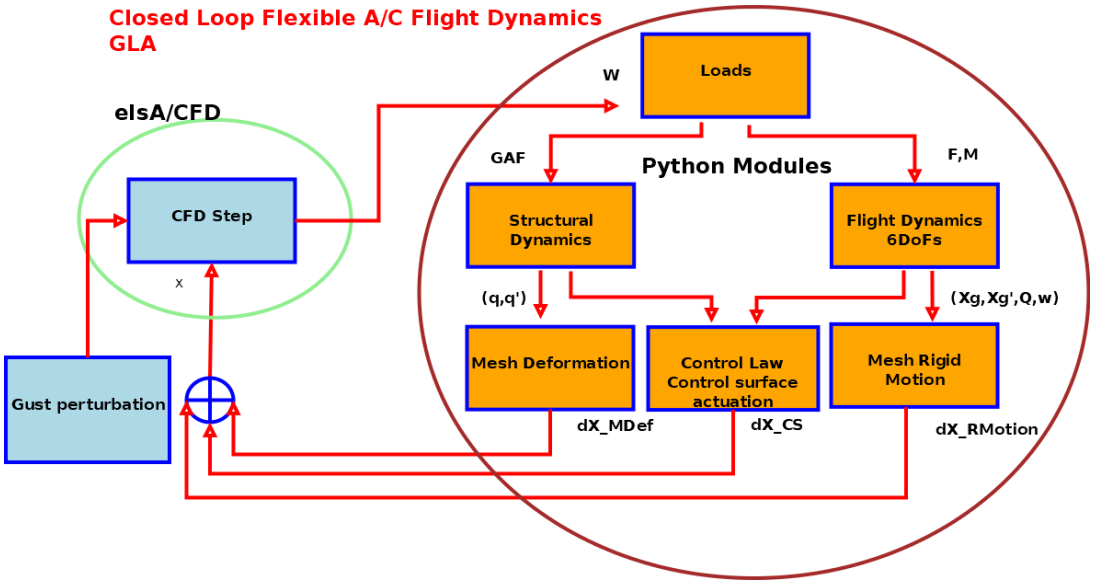

Figure 5 : Modular coupling scheme for gust response in closed loop

A gust perturbation model is available in elsA. Additional wind perturbations due to academic gust are implemented using additional grid velocities (Dequand [13]). In this paper, the (1-cos) certification gust model is used in the application section.

The gust encounter induces a perturbation from the static trim equilibrium of the flexible aircraft. Aerodynamics loads are modified and generates a variation in global forces and moments and generalized forces. These loads are delivered to the modal structural dynamics and 6DoFs flight dynamics Python modules in charge of computing the new state of the aircraft, including generalized coordinates. These data are processed by a control law module able to define the control surface command. The state of the aircraft defines the rigid motion of the grid in the inertial frame, and mesh deformation is applied to take into account modal deformations and control surface actuation. The new mesh is then returned back to the elsA solver, for the next step of the coupled simulation. In this paper, a short time step has been implemented for the simulations, allowing for a single loop iteration of the coupling process (as already stated in §2.2 a controlled convergence of the coupled process should implement a fixed-loop at this stage, but during the MAJESTIC project, the needed features were not yet available)

6 APPLICATION TO THE XRF1 MODEL OF PROJECT MAJESTIC

6.1 Presentation of the model

The XRF1 model provided by Airbus in the frame of MAJESTIC is a research model of a two-engine long range aircraft of 70 m span. Its aspect ratio is about 12. A finite-element mesh has been provided and CAD data allowed generating a suitable multiblock structured grid for elsA.

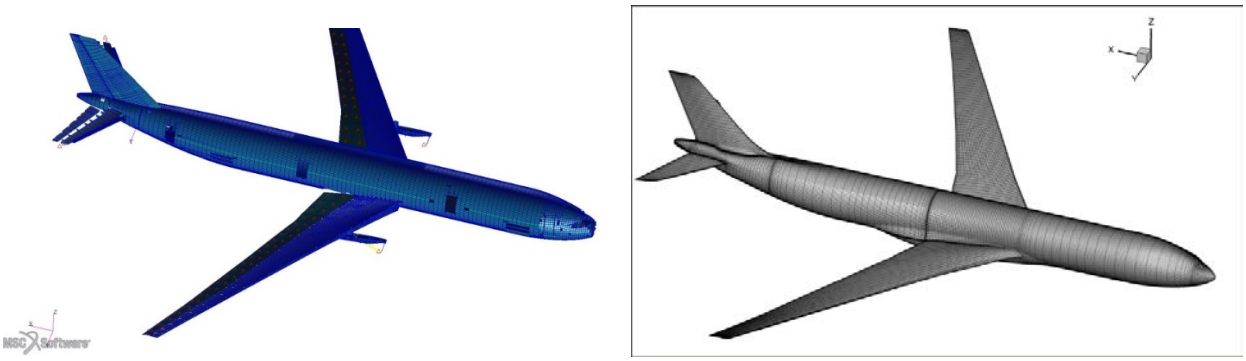

Figure 6 :MAJESTIC XRF1 AR12 Model. FE mesh (left), Aerodynamic surface grid (right)

The finite element model implements fuselage, wing, empennage including HTP and VTP and engine pods (Figure 6, left). Control surfaces at wing leading edge are modeled, as well as those of the empennage. The wing box is modelled using shell elements for spars, ribs and skins, using anisotropic MAT2 material properties. Mass properties are defined using CONM2 concentrated mass elements. The original CFD grid used for aerodynamic performance analyses is a multiblock structured one, of about 40 million cells for the half configuration. For the present flexible flight dynamics simulations, a coarser mesh has been derived and symmetrized to get a full (right+left) mesh of 12 million cells (Figure 6, right). Engines are not represented in the aerodynamic model (which could indeed introduce here a mis-estimation of trim conditions).

6.2 elsA solver aerodynamic numerics

The unsteady CFD simulations are run using the elsA solver in URANS formulation, using the Spalart-Allmaras turbulence model. The Jameson centered spatial scheme is implemented, with numerical dissipation parameters χ_2=0.5 and χ_4=0.016. The dual time stepping scheme is used for the dynamic resolution of the fluid equations, along with the backward Euler scheme for the pseudo-time loop interation at CFL 25. The physical time step is 1/500. s. 2500 iterations are computed, corresponding to a physical duration of the simulation of 5s.

The simulations are run in parallel over 48 processors. The typical duration of the unsteady flight dynamics simulations is roughly 40000 s (~11 h wall clock)

6.3 Structural model basis

As discussed previously, the structural behavior of the model is assumed to stay linear. Therefore, deformations are projected on the free-free modal basis. For the simulations presented in the paper, we focus on the so-called F1GT mass configuration of the XRF1 model, which corresponds to a cruise case configuration. The normal mode analysis is performed using MSC NASTRAN as structural solver.

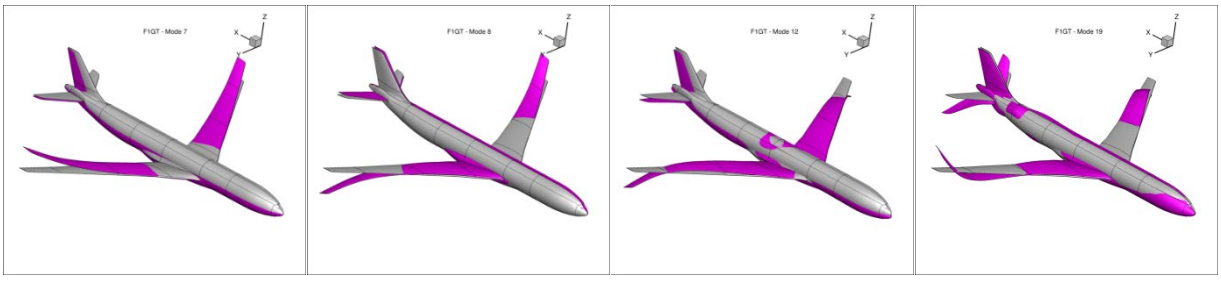

Figure 7 : Free-free flexible modes #7, #8, #12, #19 of the F1GT mass configuration

The frequency of the first flexible mode (#7) is at about 1 Hz, whereas 11 flexible modes (up to #17) have a modal frequency under 3 Hz (Figure 7). In the following simulations, the free-free modal basis has been truncated to mode #19, implementing 13 flexible modes.

6.4 Control surfaces deformation modes

Mesh deformation modes are generated on the XRF1 configurations for a set of control surfaces: stabilizer, horizontal tail plane, rudder, and internal and external ailerons (Figure 8).

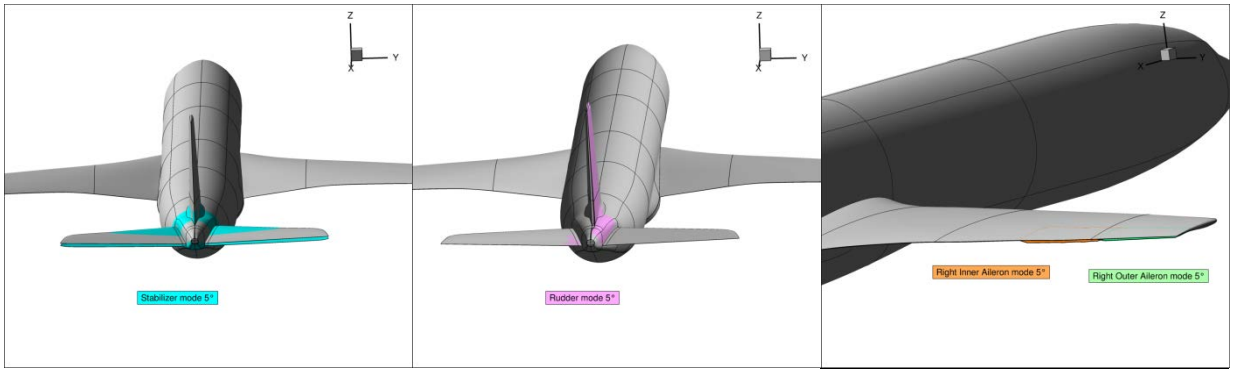

Figure 8 : Control surfaces actuation deformation modes : stabilizer (left), rudder (center) ailerons (right)

6.5 Static Trim

The dynamic system procedure described in §3 for static trim resolution is applied in the case of the XRF1 model, for F1GT mass configuration at M=0.85. The physical time duration of the simulation is 2 seconds, whereas masses and damping values are tuned to get a characteristic frequency f_{tgt}=2 Hz and an aperiodic behavior of the dynamic system. Figure 9 presents an overview of the evolution of the body axes, aerodynamic field and structural deflection during the convergence of the trim simulation towards steady state. The simulation is restarted from a static simulation at jig shape (left image) and converges to the trimmed static equilibrium illustrated by the final deformation and pressure field of right image.

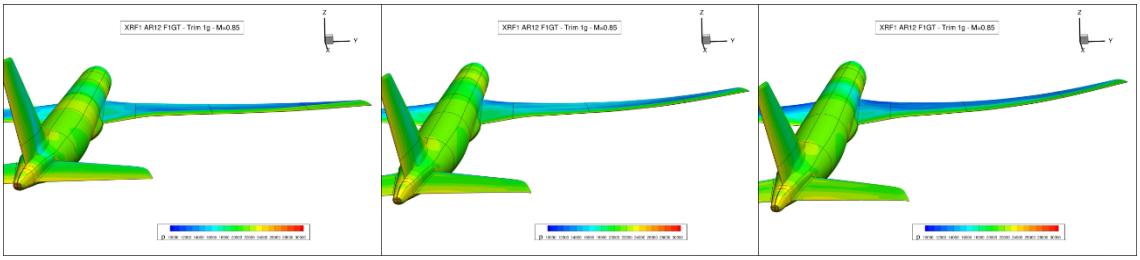

Figure 9 : XRF1 Model F1GT trim at M=0.85: initial, intermediate, final states

Aircraft angle of attack and stabilizer deflection angle in degree are displayed in Figure 10, left and global force and moment at center of gravity in the inertial axes in Figure 10, right. The flexible behavior is depicted in Figure 11. The left image presents the generalized coordinates history and the right image, the generalized forces. The time histories of all variables exhibit a good convergence towards steady state. A deflection of about 5° nose-down of the stabilizer is necessary to get a 2.2° angle of attack at trimmed conditions. Due to the symmetrical loads generated by the trim simulations for a (quasi-)symmetrical configuration, only symmetrical modes are triggered.

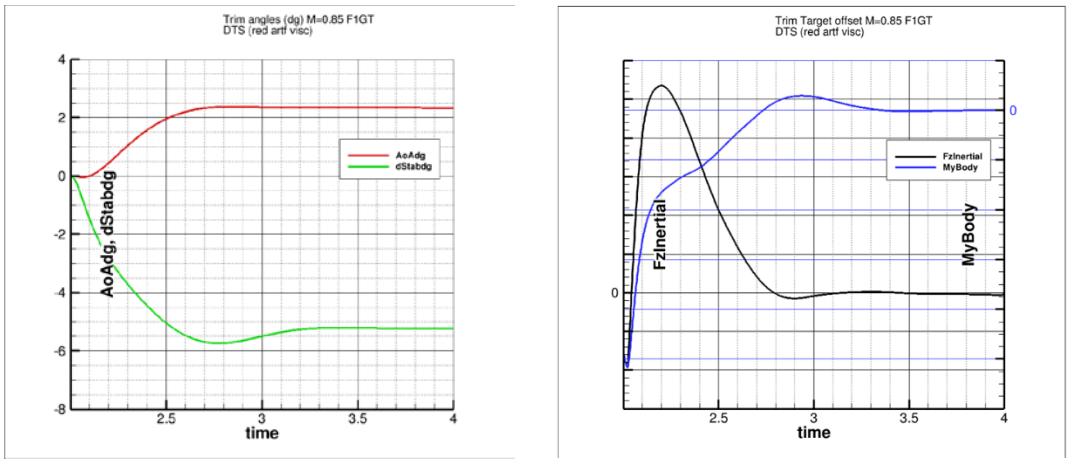

Figure 10 : XRF1 Model F1GT trim at M=0.85: trim variables and load offsets history

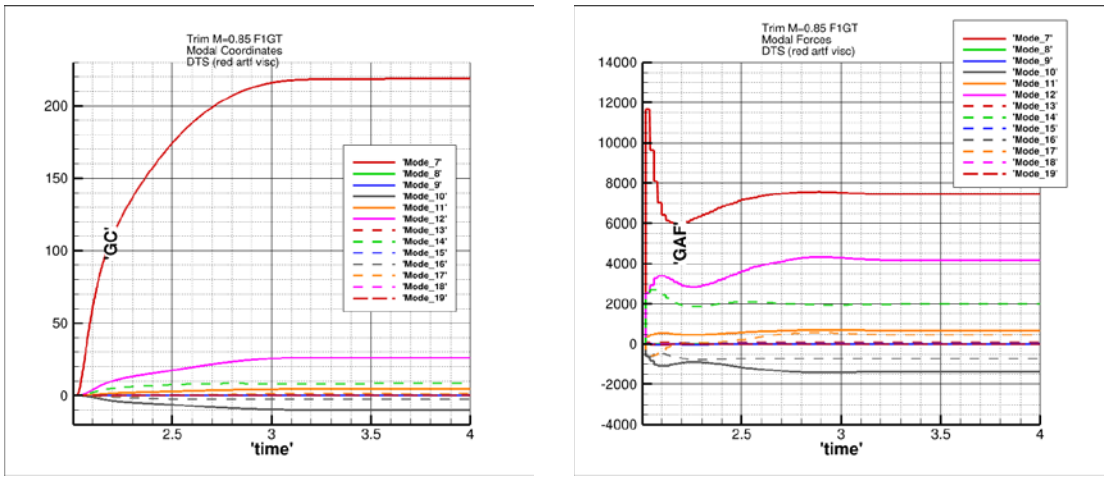

Figure 11 : XRF1 Model F1GT trim at M=0.85: Generalized coordinates and forces (Note that force/moment labels have been removed for confidentiality reasons)

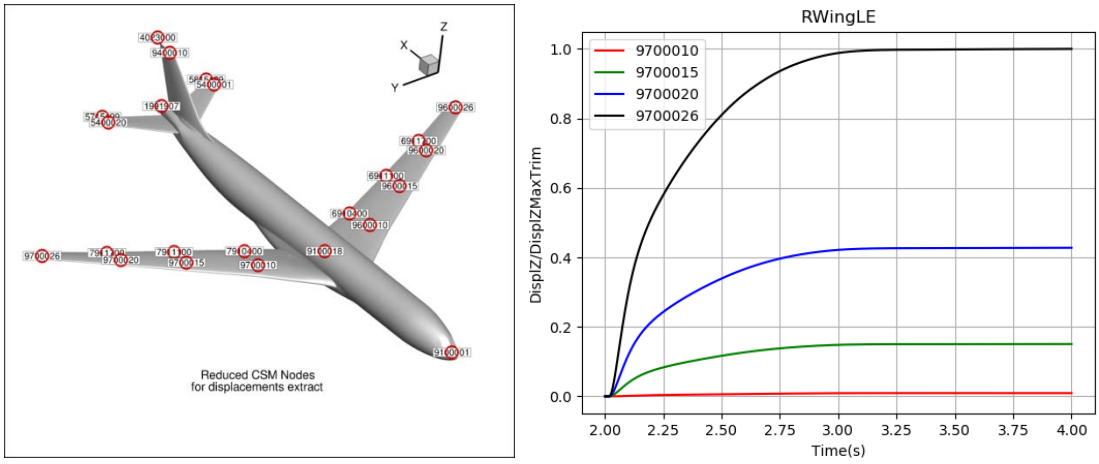

Figure 12 : XRF1 Model F1GT trim at M=0.85: Location of structural grid nodes sensors (left) Vertical displacement convergence of right wing structural grid nodes, reduced by max wing tip LE displacement, wing tip LE in black (right)

The main contribution to wing deflection is associated with mode #7, corresponding to first symmetrical bending mode, the second one corresponds to mode#12 (second symmetrical bending mode). The computed overall vertical displacement at wing tip leading edge is about 4.5 m in this case (Figure 12, right).

6.6 Maneuver: prescribed rudder actuation

A number of unsteady flexible flight dynamics simulations have been performed in the F1GT mass case at M=0.85 in open loop. Actuations of control surfaces have been simulated, coupled with the resolution of the flexible flight dynamics equations. The effect of the deflection of rudder, HTP control surface, and internal and external ailerons in symmetrical or single-side actuation has been computed, in order to generate an aerodynamic model of the flexible aircraft. We present here the case of the actuation of the rudder during 2 s, following a S-shaped function in time, with an amplitude of 7°.

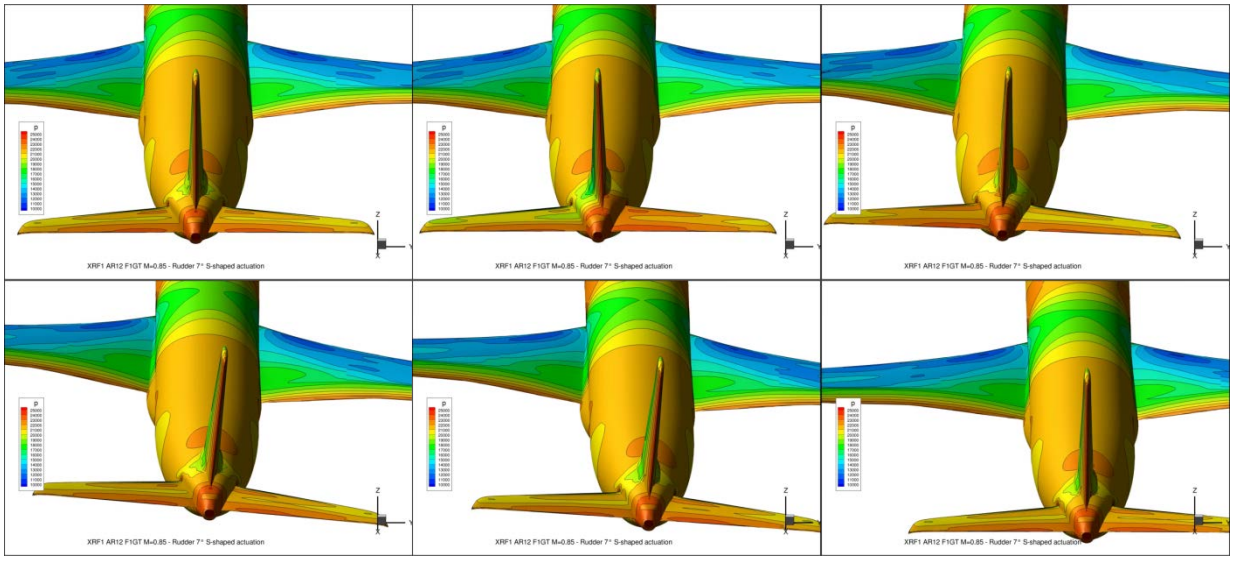

Figure 13 : XRF1 Model F1GT: S-shaped rudder of 7° amplitude actuation: pressure field and motion of the aircraft during maneuver (0.5 s between two views)

The simulation duration is 5 seconds of physical time. In Figure 13, we show an rear view of the effect of the actuation of the rudder on the trajectory of the aircraft and on the pressure load at 6 instants of the simulation. The S-shaped actuation function used is shown in Figure 14, left.

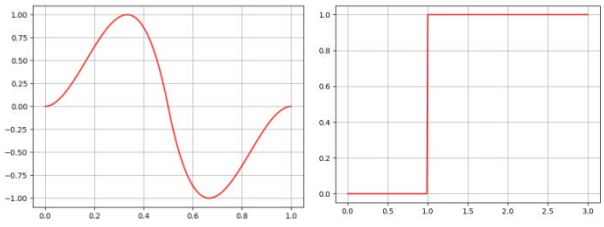

Figure 14 : S-shaped and step actuation functions

As expected, the actuation of the rudder to the right generates first the occurrence of a positive yaw moment M_z during one second (Figure 16, right), which induces a yaw motion to the right (Figure 15, left). Then, the roll moment M_x comes back to a positive value, inducing a roll motion of the aircraft (up to 5°, Figure 15, center), while the yaw moment becomes negative, getting the aircraft to come back by the end of the simulation to near zero roll and yaw angles.

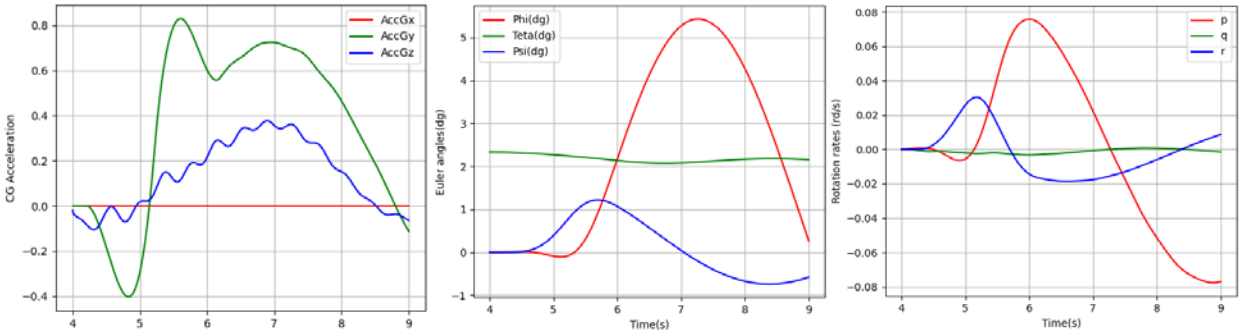

Figure 15 : XRF1 Model F1GT: S-shaped rudder of 7° amplitude actuation: Flight dynamics data during maneuver: CG acceleration in inertial axes (left), Euler angles (center), rotation rates (right).

However, the simulation duration is not sufficient to reach the steady state after maneuver, as shown by the final evolution of Euler angles and rotation rate in Figure 15. The lateral acceleration of the center of gravity is first negative and then reaches a positive value of 0.8 m/s^2 after 1.5 s. A maximum vertical acceleration of 0.4 m/s^2 is obtained after 3s (Figure 15, left). The contribution of flexibility to vertical acceleration is clearly visible in this figure, leading to a certain waviness of the curve, related to modal frequencies.

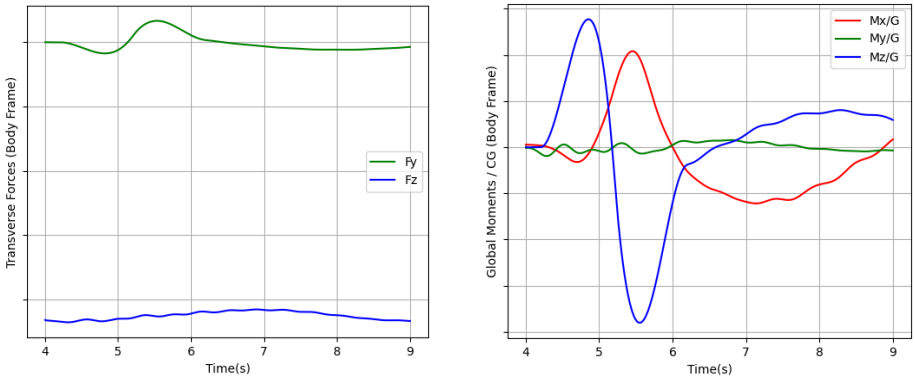

Figure 16 : XRF1 Model F1GT: S-shaped rudder of 7° amplitude actuation: Aerodynamic loads in body axes: Transverse forces (left), moments wrt to CG (right). (Note that force/moment labels have been removed for confidentiality reasons)

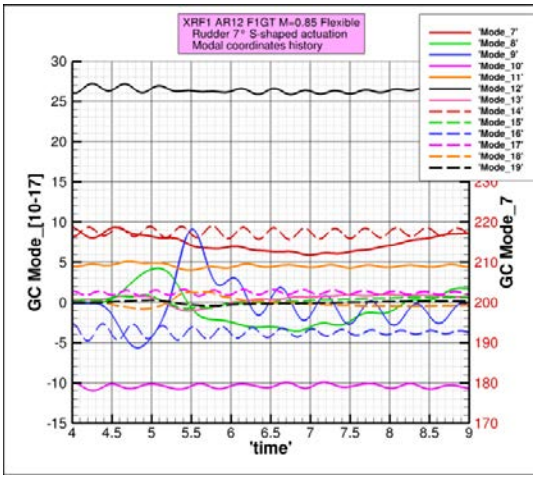

Figure 17 : XRF1 Model F1GT: S-shaped rudder of 7° amplitude actuation: modal coordinates histories

Figure 17 depicts the evolution of modal coordinates during the simulation. Contrary to the symmetrical trim case (Figure 11), the whole modal basis is activated, due to the non symmetrical loads generated by the maneuver. The most solicited modes are anti-symmetric (mode#8 and mode #9), but mode#7 (symmetrical first bending) is also triggered at low frequency. As indicated before, all the modes embedded in the simulation basis have a low frequency under 3 Hz, which leads to the unsteady wavy response of the structure.

6.7 Gust response: open loop and closed loop. GLA

The aim of this section is to show the ability of CFD to simulate gust load alleviation using specifically designed control laws.

6.7.1 Aeroelastic model identification

The first step for the design of the control law is to generate an aerodynamic model of the flexible aircraft. This has been done in the case of the F1GT mass configuration of the XRF1 model at M=0.85. Several flexible flight dynamics simulations have been run in open loop:

- AILINR : Response to a 7° amplitude deflection step (Figure 14, right) of internal right aileron,
- AILOUTR : Response to a 7° amplitude deflection step of external right aileron,
- AILOUTRL : Response to a 7° amplitude deflection step of both external aileron
- HTP : Response to a 5° amplitude deflection step of the HTP control surface
- VTP : Response to a 7° amplitude deflection step of the rudder
- GUST: Response to (1-cos) certification gust, of wavelength 100m, vertical gust speed 5 m/s.

A complete set of numerical data is extracted from each simulation, including:

- position, velocity and acceleration of the center of gravity (CG);
- body axes (Euler angles) and rotation rates;
- angle of attack and side slip;
- global aerodynamic force and moment wrt to CG in body and inertial axes;
- right wing only aerodynamic force and moment wrt to CG in body axes;
- physical displacement in body axes of selected structural nodes (Figure 12, left);
- generalized modal forces and coordinates.

This data set is used to generate a reduced-order model of the aircraft to feed the control synthesis problem for gust load alleviation which is described in the next section.

From a control perspective, the gust load alleviation problem is a disturbance rejection problem aimed at decreasing the maximum bending moment when subject to some disturbance gust using some sensors and actuators. Indeed, reducing the bending moment is a key player for reducing the wing box mass.

Following the notations of the standard control form (Zhou [14]), the bending moment is called a performance output, denoted z, and the gust is called an exogeneous input, denoted w. Control input and measurement output are denoted u and y, respectively. Choice of actuators and sensors is crucial in control, yet this is a task which is complex to perform in a systematic way and it is therefore often done manually based on physical considerations. Here, the whole set of data presented above has not yet been fully exploited and sensors/actuators have been arbitrarily

chosen as follows: y gathers the pitch rate and vertical acceleration at CG while u is a symmetric command of the external ailerons.

With these notations, the identification step is aimed at finding a linear model under the form:

$$\begin{cases} \dot{x} = Ax + B_w w + B_u u \\ z = C_z x + D_{zw} w + D_{zu} u \\ = C_y x + D_{yw} w + D_{yu} u \end{cases} \qquad (6.7.1)$$

where x is the internal state of the model (which does not necessarily have an explicit physical interpretation).

The identification process is in three steps here: first, an initial large model is obtained directly from the time-domain data with a black-box method called matrix pencil method (Yingbo [15]). This initial model can be unstable and this issue is alleviated by projection onto a stable Hoo subspace (see Glover [16]). The resulting large stable model is finally reduced using the Loewner frequency-domain interpolation approach (Mayo [17]). The resulting model is denoted H_r and its response (plotted in red) is compared to the initial time-domain data in Figure 18. Note the mismatch in the first (sizing) peak of the wing root bending moment. This could certainly be reduced further and may lead to better control performances.

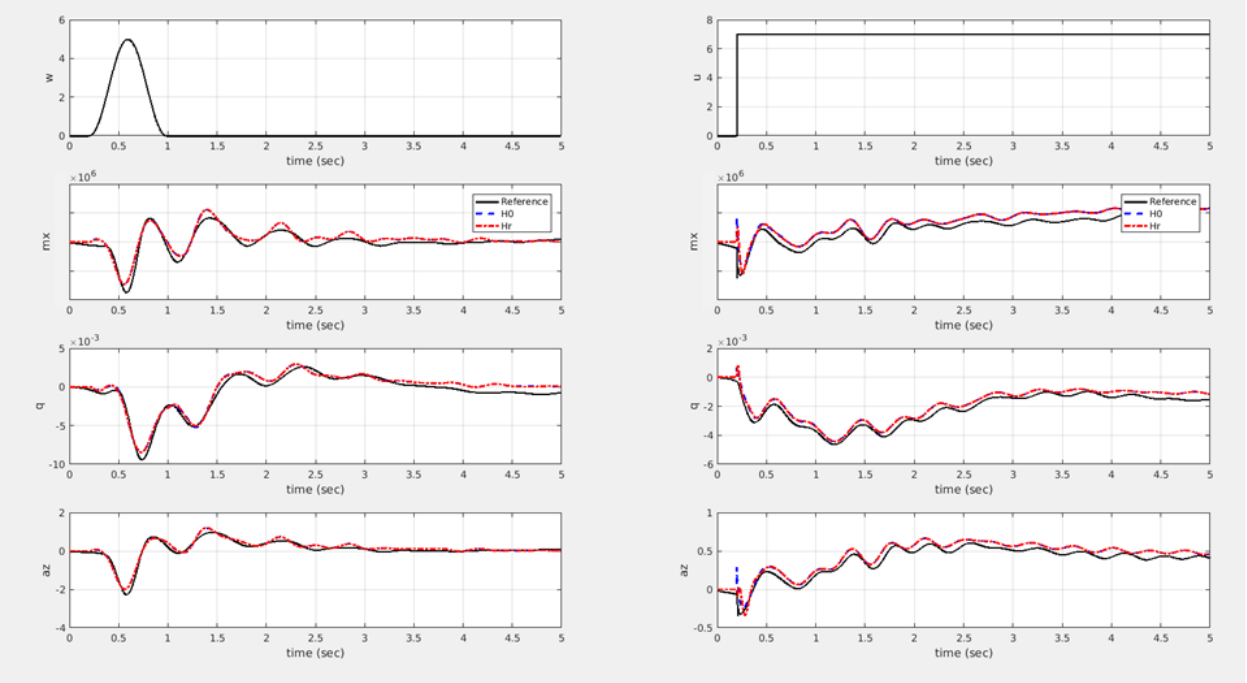

Figure 18 : Open loop identification: gust response (left), response to aileron step deflection (right) – Input signal (1st row), Bending moment (2nd row, moment labels removed for confidentiality reasons), pitch rate (3rd row), CG vertical acceleration (4th row)

6.7.2 Law control design

Based on the reduced model H_r of the flexible aircraft, a linear control law described by its state-space formulation:

$$\begin{cases} \dot{x_c} = A_c x_c + B_c y \\ u = C_c x_c \end{cases} \qquad (6.7.2)$$

is synthesized following the process detailed in (dos Reis [18]).

In addition to its performance objective to decrease the wing root bending moment, the control law must also comply with a set of constraints that would be found on a real aircraft. In particular, the law must stabilize the closed-loop, be stable, be structured (i.e. of low dimension D_c=0 here) and leave untouched low frequencies (to preserve handling qualities) and high frequencies (for robustness). These constraints are important to consider in order to avoid exhibiting unrealistic performance. In practice, the problem is solved using the structured Hoo synthesis framework (Apkarian [19]) available in MATLAB with routines *hinfstruct* or *systune*. The state-space matrices A_c, B_c, C_c are then extracted and integrated in a Python module dedicated to the resolution of the dynamic system 6.7.2.

6.7.3 GLA

In this section, 3 simulations are compared in order to analyze the impact of flexibility during gust and to validate the Gust Load Alleviation (GLA) induced by the designed control law:

- Open-loop gust response of the rigid aircraft
- Open-loop gust response of the flexible aircraft
- Closed-loop gust response of the flexible aircraft with controlled ailerons (Figure 23).

The closed-loop simulation environment is the one plotted in Figure 5. Figure 19 presents a comparison of the 3 simulations in terms of pitch rate, vertical CG acceleration and right wing bending moment. The first indication is that flexibility reduces peaks values for all three variables. In particular, a 20% reduction is observed on the bending moment (Figure 19, right plot, Figure 21). Moreover, the control induces a reduction of 10% of the bending moment offset to steady trimmed values, compared to open-loop flexible results.

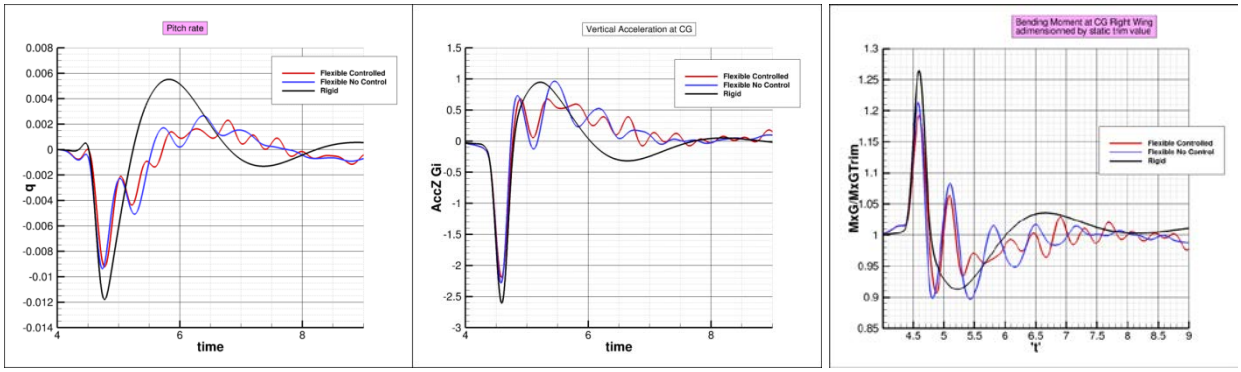

Figure 19 : Comparison of gust response: pitch rate (left), vertical CG acceleration (center), right wing bending moment reduced by static trim value (right). Rigid case in black, open-loop flexible in blue, closed-loop flexible in red

Vertical Acceleration at CG	Steady	min	max	amplitude
FlexVSRigidGLA(Absolute)		-12,39%	1,74%	-8,62%
ControlVsFlexGLA(Absolute)		-3,92%	-29,25%	-11,44%
FlexVSRigidGLA(DeltaToSteady)		-12,46%	1,71%	
ControlVsFlexGLA(DeltaToSteady)		-3,95%	-28,84%	

Figure 20 : GLA figures for CG vertical acceleration

Bending Moment Half Right Wing	Steady	min	max	amplitude
FlexVSRigidGLA(Absolute)		-4,06%	-1,69%	-10,21%
ControlVsFlexGLA(Absolute)		-1,75%	1,04%	-9,69%
FlexVSRigidGLA(DeltaToSteady)		-19,40%	17,66%	
ControlVsFlexGLA(DeltaToSteady)		-9,97%	-9,12%	

Figure 21 : GLA figures for right wing bending moment

In terms of vertical CG acceleration alleviation, a minor 4% reduction is obtained in the flexible case with control in the first negative peak, but 30% reduction at positive second peak after 1.5 s (Figure 19, center, Figure 20).

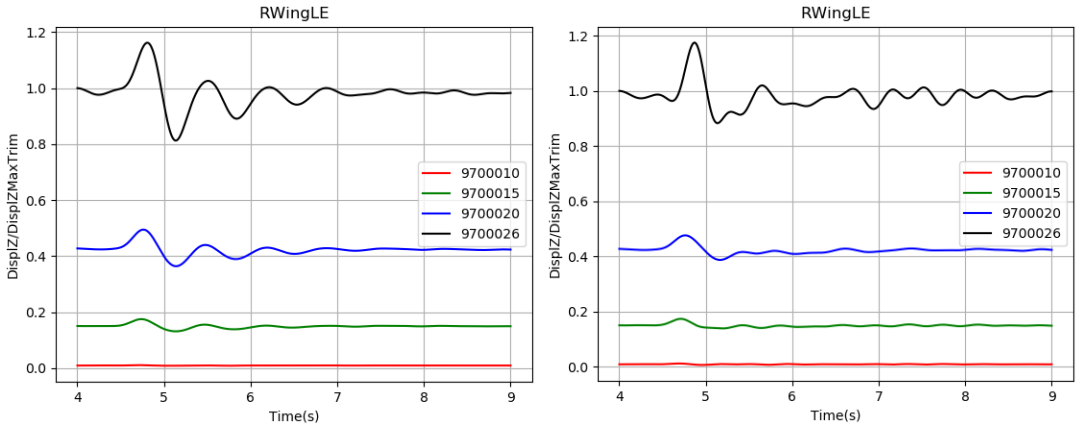

Figure 22 : Reduced vertical displacement of right wing structural grid nodes, without control (left), with control (right), wing tip LE in black

Figure 22 shows a comparison of the vertical deformation of the wing leading edge at 4 stations in span, in the flexible open-loop and closed-loop cases. The black curves correspond to the wing tip leading edge node (9700026). The values are reduced by the static trim vertical displacement at this node. The peak-to-peak deflection is clearly reduced in the controlled case, but the maximum deflection of the wing doesn't seem to be reduced. However, further oscillations seem to be damped more rapidly.

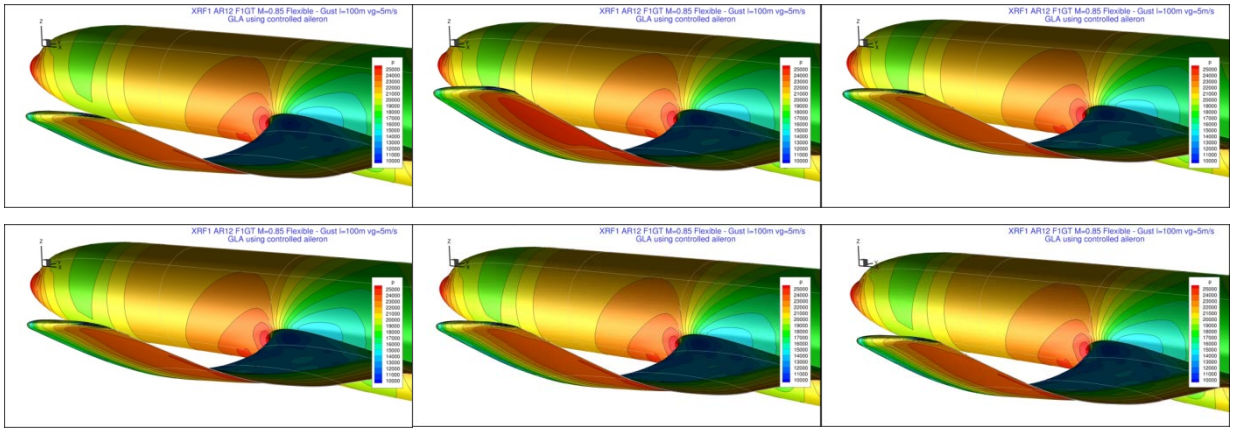

Figure 23 : XRF1 controlled gust response : oveview of wing deformation and aileron deflection during gust encounter (0.5 s between two views)

7 CONCLUSIONS

Due to environmental constraints, next generation long range aircrafts are bound to have larger aspect ratio wings, a more flexible structure and they will face more complex aeroelastic issues. In this paper we have presented a methodology to solve flight dynamics problems of flexible aircraft using CFD. This methodology is based on the use of a modular framework implementing the elsA CFD solver in externalized mode, coupled with external Python modules in charge of solving the flight dynamics behavior of the aircraft along with the structural dynamics equations. Mesh deformations tools are implemented to take into account modal deformation of the structure and control surfaces actuation. Selected open loop applications have been shown in the case of the Airbus XRF1 model implemented in the French DGAC funded project MAJESTIC. Trim simulations of the flexible aircraft have been presented in static, and an example of maneuver due to rudder actuation has been detailed. A full CFD flight dynamics data base has been collected to analyze the response to the actuation of the aircraft control surfaces. The capability of this methodology to address closed-loop problems in implementing control laws has been shown and applied to the case of the application to Gust Load Alleviation CFD simulations.

However, some assumptions used in this paper should have to be released in future works. In particular, non-linear large displacements have to be modelled, which could require either the coupling with a non-linear structural solver at least in static, or the generation and use of reduced order models of the non-linear structure. In this case, the assumption of constant inertia matrix should also have to be reconsidered. A proper validation of these methods is planned in the next future in the frame of the DGAC funded ALFA project, by the exploitation of flight tests of the XWing Airbus demonstrator. Another topic of interest will be the integration of a flutter control law, and the related closed loop simulations using CFD. Eventually, the robustness of the approach will be increased by the integration of the developed Python tools in the MIMAS aeroelastic toolbox currently developed at ONERA. This will pave the way for a larger use of the methodology by enabling the capability of coupling it with the next generation CFD solvers CODA and Sonics.

ACKNOWLEDGEMENTS

The authors gratefully acknowledge the financial support provided in the project MAJESTIC by French DGAC and the European Union and the fruitful collaboration with Airbus during the project.

REFERENCES

[1] R. Palacios, C E.S. Cesnik, « Dynamics of Flexible Aircraft”
Cambridge University Press, June 2023, https://doi.org/10.1017/9781108354868
Github : https://github.com/ImperialCollegeLondon/flexibleaircraftbook

[2] N. Nguyen, I. Tuczu, “Flight Dynamics of Flexible Aircraft with Aeroelastic and Initial Force Interactions” AIAA Atmospheric Flight Mechanics Conference August 2009, Chicago, Illinois - https://doi.org/10.2514/6.2009-6045

[3] J. Murua,H. Hesse, R. Palacios, J.M.R. Graham « «Stability and Open-Loop Dynamics of Very Flexible Aircraft Including Free-Wake Effects”, AIAA/ASME/ASCE/AHS/ASC Structures, Structural Dynamics and Materials Conference April 2011 ,Denver, Colorado https://doi.org/10.2514/6.2011-1915

[4] V.Portapas, A. Cooke, M.Lone, “Modelling framework for flight dynamics of flexible aircraft” Aviation, 2016 Volume 20(4): 173-182 , doi:10.3846/16487788.2016.1264719.

[5] R.Heinrich, L.Reimer, "Comparison of Different Approaches for Gust

Modeling in the CFD Code TAU", IFASD 2013, Bristol (UK) 24-26 June 2013.

[6] M. Ritter, M.S. Roeser, L. Reimer, "CFD-based Multi-Axis Maneuver Simulation for System Identification of Flexible Transport Aircraft", AIAA 2020-2125,AIAA SciTech Forum, 6-10 January 2020, Orlando, FL

[7] L.Cambier, V.Gleize, J.Mayeur, “Verification and validation of the ONERA elsA flow Solver on RANS benchmark” AIAA 2014-0239, Scitech, 13-17 January 2014, National Harbor, MarylandSession, https://doi.org/10.2514/6.2014-0239

[8] L.Cambier, “Advanced Numerical Simulation in Computational F luid Dynamics and Multiphysics at ONERA: Issues, Results and Strategy”, 53rd 3AF International Conference on Applied Aerodynamics 26 – 28 March 2018, Salon de Provence, France

[9] A. Dugeai, Y. Mauffrey, A.Placzek, S.Verley, “Overview of the Aeroelastic Capabilities of the elsA Solver within the Context of Aeronautical Engines”, AerospaceLab Journal, Issue 14, September 2018

[10] B. Isnard, G. Tanguy, D. Farcy, A. Dugeai, E. Garnier, J-M Foucaut, "Comparison of Numerical Reduced Order Models of a Generic UCAV Configuration using a New Displacement Grid Method", AIAA 2023-3269, June 2023, AIAA Aviation 2023 Forum, https://doi.org/10.2514/6.2023-3269.

[11] Caughey D.A., “Introduction to Aircraft Stability and Control. Course Notes for M&AE 5070”, Sibley School of Mechanical & Aerospace Engineering Cornell University, Ithaca New York 14853-7501 2011

[12] S.M. Murman, M.J. Aftosmis, M.J. Berger, "Simulations of 6-DOF Motion with a Cartesian Method » AIAA-2003-1246, 41st AIAA Aerospace Sciences Meeting, January 6-9 2003, Reno, Nevada, https://doi.org/10.2514/6.2003-1246.

[13] S. Dequand, C. Liauzun, “Green Regional Aircraft Gust Response” Greener Aircraft Aviation, Bruxelles Octobre 2016, ONERA TP 2016-684.

[14] K. Zhou, J. C. Doyle, and K. Glover, . "Robust and optimal control." *Prenticel Hall*. 1996.

[15] H. Yingbo, and T. K. Sarkar. "Matrix pencil method and its performance". *International Conference on Acoustics, Speech, and Signal Processing*. 1988.

[16] K. Glover. "All optimal Hankel-norm approximations of linear multivariable systems and their L,∞-error bounds." *International journal of control*. 1984.

[17] A.J. Mayo and A.C. Antoulas. "A framework for the solution of the generalized realization problem." *Linear algebra and its applications*. 2007.

[18] A. dos Reis de Souza, P. Vuillemin, C. Poussot-Vassal, D. Quero, “Gust load alleviation using reduced-order aeroelastic models and observer-based robust control.” Journal of Guidance, Control and Dynamics, Vol 46, N° 5, May 2023. https://doi.org/10.2514/1.G007153

[19] P. Apkarian, and N. Dominikus. "Nonsmooth H∞ synthesis." *IEEE Transactions on Automatic Control*. 2006.